LAWRENCE
LIVERMORE
NATIONAL
LABORATORY

LLNL-JRNL-648039

7 A resolution in protein 2D-crystal X-ray diffraction at LCLS

B. Pedrini, C. Tsai, G. Capitani, C. Padeste, M. Hunter, N. Zatsepin, A. Barty, W. H. Benner, S. Boutet, G. Feld, S. P. Hau-Riege, R. A. Kirian, C. Kupitz, M. Messerschmitt, J. I. Ogren, T. Pardini, B. Segelke, G. J. Williams, J. C. Spence, R. Abela, M. Coleman, J. Evans, G. Schertler, M. Frank, X. Li

December 19, 2013

Philosophical Transactions of the Royal Society B

Disclaimer

7 Å resolution in protein 2D-crystal X-ray diffraction at LCLS

Bill Pedrini*[1], Ching-Ju Tsai[1], Guido Capitani[1], Celestino Padeste[1], Mark S. Hunter[2], Nadia A. Zatsepin[4], Anton Barty[5], W. Henry Benner[2], Sebastien Boutet[6], Geoffrey K. Feld[2], Stefan P. Hau-Riege[2], Richard A. Kirian[5], Christopher Kupitz[4], Marc Messerschmitt[6], John I. Ogren[7], Tommaso Pardini[2], Brent Segelke[2], Garth J. Williams[6], John C. H. Spence[4], Rafael Abela[1], Matthew Coleman[2], James E. Evans[3], Gebhard Schertler[1], Matthias Frank†[2], and Xiao-Dan Li‡[1]

[1]Paul Scherrer Institute, 5232 Villigen PSI, Switzerland
[2]Lawrence Livermore National Laboratory, 7000 East Avenue, Livermore, CA, 94550, USA
[3]Environmental Molecular Sciences Laboratory, Pacific Northwest National Laboratory, 3335 Innovation Blvd., Richland, WA, 99354, USA
[4]Arizona State University, 300 E. University Dr., Tempe, AZ, 85287, USA
[5]Center for Free-Electron Laser Science, DESY, Notkestrasse 85, 22607 Hamburg, Germany
[6]Linac Coherent Light Source, 2575 Sand Hill Road, Menlo Park, CA, 94025, USA
[7]Physiscs Departement, Boston University, 590 Commonwealth Ave, Boston, MA, 02215, USA

January 10, 2014

Abstract

Membrane proteins arranged as two-dimensional (2D) crystals in the lipid environment provide close-to-physiological structural information, which is essential for understanding the molecular mechanisms of protein function. X-ray diffraction from individual 2D crystals did not represent a suitable investigation tool because of radiation damage. The recent availability of ultrashort pulses from X-ray Free Electron Lasers (X-FELs) has now provided a mean to outrun the damage. Here

*Corresponding author. e-mail: bill.pedrini@psi.ch
†Corresponding author. e-mail: frank1@llnl.gov
‡Corresponding author. e-mail: xiao.li@psi.ch

we report on measurements performed at the LCLS X-FEL on bacteriorhodopsin 2D crystals mounted on a solid support and kept at room temperature. By merging data from about a dozen of single crystal diffraction images, we unambiguously identified the diffraction peaks to a resolution of 7 Å, thus improving the observable resolution with respect to that achievable from a single pattern alone. This indicates that a larger dataset will allow for reliable quantification of peak intensities, and in turn a corresponding increase of resolution. The presented results pave the way to further X-FEL studies on 2D crystals, which may include pump-probe experiments at subpicosecond time resolution.

Keywords. 2D protein crystal, X-ray diffraction, X-ray Free Electron Laser, Crystallographic data analysis, Bacteriorhodopsin

1 Introduction

Knowledge of the atomic structure of membrane proteins, especially the structural changes triggered by external stimuli [1, 2], is of keen interest. A two-dimensional (2D) protein crystal is a 2D periodic array of the same motif, forming a single layer of molecules. This is a favorable arrangement for membrane proteins, because the lipidic component between the proteins closely mimicks the natural environment in the cell membrane [3]. Moreover, it can be assumed that the structure in the 2D crystal environment is almost the same as in the natural state, and that potential structural changes are not as restricted as it may happen in 3D crystals [4].

Since the 1970s, Electron Microscopy (EM) has exploited the signal enhancement brought about by the 2D periodic structure and provided a few dozen of unique structures with resolution below 1 nm [5, 6, 7]. The key of that success is that, unlike in diffraction-type experiments, both amplitude and phase of the Bragg reflections are experimentally accessible (see for example [8]). Continuous methodological improvements [9, 10, 11] that include, in particular, cryo-cooling of the sample [12] have led to structures at atomic resolution [13]. However, a real breakthrough in terms of high-throughput has always been hampered by radiation damage.

The situation is even more critical with X-rays, for which the ratio between useful diffraction and damaging absorption events is by far worse [14]. Until the advent of X-ray Free Electron Lasers (X-FELs) [15, 16], the experiments were limited to powder diffraction in transmission from pelleted bacteriorhodopsin (bR) 2D crystals [17], and to grazing-incidence diffraction from bR 2D crystals floating at the water-air interface [18]. While X-ray diffraction from a single 2D crystal would offer remarkable advantages, synchrotron sources are limiting, in that radiation damage destroys the sample faster than the accumulation of sufficient signal in the Bragg peaks. At X-FELs the situation is radically different: diffract-before-destroy experiments in the framework of Serial Femtosecond Crystallography (SFX) [19] on submicrometer-sized 3D crystals have recently proven that the femtosecond X-FEL pulses outrun the damage, and that they are of sufficient intensity to generate meaningful Bragg peak signals. The above results prompted us to extend the application of the diffract-before-destroy concept to 2D protein crystals under close-to-physiological conditions of hydration and temperature, thus avoiding the

deleterious effects of cryogenic cooling. Further considerations in support of this approach were related to the stronger penetration power of X-rays, which possibly allows the acquisition of diffraction data at larger tilt angles than feasible with cryo-EM, as well as to the perspective of exploiting the finite size of the 2D crystal in the direction perpendicular to the crystal plane for direct phase retrieval [20], not possible in standard 3D crystallography.

Even though the single-layer arrangement strongly reduces the scattering power of 2D crystals, the feasibility of diffract-before-destroy experiments was demonstrated during an LCLS beamtime at the Coherent Diffraction Imaging (CXI) station in May 2012, where we captured sub-nanometer Bragg diffraction from individual 2D crystals [21]. The submicrometer sized X-ray focus available at CXI enhanced the probability of simultaneously illuminating only a small number of 2D crystals. However, during this initial beamtime, the single-crystal hit-rate was so low that averaging data for a complete sampling of all Bragg peaks was impossible. Thus, the attainable resolution remained signal-to-noise limited, which affected the overall interpretability of the achieved results.

Here, we describe a larger dataset acquired in May 2013, and show that a key point is to merge data from different crystals to enhance the signal-to-noise ratio of the measurable Bragg reflections. Although limited by the small number of analyzable diffraction images, our approach led us to conclude that the prepared sample diffracts to at least 7 Å, and indicates that reliable determination of the reflection intensities just requires more diffraction patterns.

2 Methods

2.1 X-ray diffraction measurements

The measurements were performed at the 0.1 μm focus environment of the CXI experimental station of the LCLS X-FEL [22], at an X-ray wavelength of 8.8 keV (1.4 Å) and with nominal pulse energies of about 2 mJ.

The sample was supported by a solid silicon wafer, shaped with an extended array of 100×100 μm^2 thin windows consisting of a 5 nm carbon film with a 40 nm PMMA layer. 2.2 μg bR 2D crystals, with a typical size of 0.5-1.0 μm, were suspended in 15 μl of 0.5 % w/v glucose solution. This was painted on the backside part of the wafer, so that it could adhere to the carbon face of the windows. After drying, the remaining layer of glucose acted as protection against dehydration in the vacuum chamber.

The X-FEL was run in "burst mode", and the wafer was moved transversely to the beam so that every X-ray pulse hit a new, undamaged window. In this way, the effective rate of diffraction image acquisition was about 1 Hz.

2.2 Diffraction image analysis

For a 2D crystal, the X-ray cross-section is markedly different from zero only around the Bragg rods. These are lines perpendicular to the 2D crystal plane. Their projection onto this plane correspondst to the reciprocal lattice of the 2D crystal lattice. Each rod is therefore labeled by indices (h, k) corresponding to the two reciprocal unit cell vectors (a_*, b_*). Peaks in 2D crystal diffraction images originate from the intersection of the Ewald sphere with the Bragg rods, thus are labeled with the same indices pair. In

the simplest approach, we considered only the images which exhibited a clear diffraction pattern from a single 2D crystal, with the crystal plane almost perpendicular to the incoming beam. Such images were tagged because of the characteristic diffraction peak positions ("peak lattice"). In an individual image, only the most prominent peaks are visible. To evaluate the potential completeness of the measurable peaks, we enhanced the signal-to-noise ratio by averaging the intensities of small sectors of diffraction images, with the sectors centered at the position of equivalent peaks. This allowed us in particular to merge data from different images. To do that, however, we needed 1) to precisely determine the orientation of each peak lattice, which was possible based on the positions of the most prominent peaks and 2) to index each lattice, which required the intensities of those prominent peaks as input, and which includes, among other, the assessement of the face of the 2D crystal exposed to the beam. The details of the protocol will be presented in a future publication.

3 Results and Discussion

The considered dataset consisted of 324 diffraction images, acquired within about 6 minutes of beamtime. Among these, 15 exhibited clear diffraction patterns originating from a single bR 2D crystal, out of which 11 were unambiguosly indexed. Figure 1 shows a typical example. The peaks are indeed positioned on an easily recognizable 6-fold symmetric pattern, originating from the two reciprocal unit cell vectors (a_*, b_*) shown in green, which in the case of the used bR sample are known to have equal length $2\pi/62.45$ Å and to form an angle of 60° [5, 10]. The red circles mark the positions of prominent peaks that were used to find the exact orientation of the peak lattice with respect to the beam axis, perpendicular to the figure.

Because of Friedel's law, for perpendicular incidence the p_3-symmetry of the 2D crystal would result in a 6-fold symmetric diffraction intensity for short incoming X-ray wavelength. This limit is not achieved within the actual experimental setup. Owing to the curvature of the Ewald sphere, the (h, k) and $(-h, -k)$ peaks are no longer Friedel pairs, which is manifest in that the symmetry of the observed peak intensities is clearly reduced from 6- to 3-fold. Crystallographically equivalent peaks are related only by a 120° rotation, meaning that peaks (h, k), $(-h-k, h)$ and $(k, -h-k)$ belong to the same equivalence class, which we label by $((h, k))$. Figure 2 displays the peaks observed for classes $((7, 1))$, $((-7, -1))$, $((1, 7))$ and $((-1, -7))$, all at 7.2 Å resolution, as magnifications of the diffraction image of Figure 1 around the concerned peak positions. The peak intensity variations within a class are in part recognisable by eye, and can be explained as the joint effect of Poisson statistics with small tilts of the individual 2D crystals. Indeed, tilts of less than 25° can hardly be assessed from the peak positions alone [23].

The 11 indexable images were further used for enhancing the peak signals. Figure 3 displays image sector sums for different equivalence classes at the maximal resolution of about 7 Å relevant within the present discussion. Each plot arises from the intensity sum of at least 20 image sectors. In this way, almost all peaks in the mentioned resolution range became observable. Peaks in the class $((1, 7))$ are clearly visible in most of the individual patterns, and therefore also emerge as prominent features in the image sector sum. In contrast, the $((-7, -1))$ and $((-1, -7))$ reflections represent typical peaks that can hardly be identified in a single diffraction image (see Figure 2), yet appear as a clear

peaks in the sum. Finally, $((7,1))$ exemplifies the few reflections being so weak that they do not emerge from noise even after the summing procedure, although one can guess that a peak-like feature is present.

At this point, we note that two overall indexing ambiguities are intrinsic and can be fixed arbitrarily. They correspond to an arbitrary choice of the reference orientation of the 2D crystal. First, exchanging $((h,k))$ and $((k,h))$ results in reverting the face of the 2D crystal exposed to the positive out-of-plane direction. We fixed this freedom in order to be consistent with the conventions used in Ref.[24]. Second, swapping $((h,k))$ with $((-h,-k))$ corresponds to a 180° rotation (equivalent to a 60° rotation) of the crystal.

From the described results, we conclude that the prepared 2D crystals diffract to at least 7 Å. A proper, complete measurement of the peak intensities will benefit from merging data from a larger diffraction image set. We are working towards using images arising from the illumination of a few 2D crystalline domains, where diffraction spots still remain well separated and therefore indexable; indeed, about 30% of the 324 images in the dataset discussed in this paper belonged to this category. From the sample preparation point of view, the aim will be to increase the percentage of indexable images, and especially to avoid powder-like rings, by tuning the protein concentration in the solution to be painted on the wafer. We also plan to optimize the shape of the X-ray focus by cutting tails in the transverse direction that weakly illuminate neighbouring 2D crystals, giving rise to a spotty, ring-like background. Finally, we expect to increase the image acquisition rate by reducing the translational motion of the stage between two subsequent image acquisitions. This may be possible by employing wafers with either smaller and closer windows, or with rectangular windows with an extended dimension, to be scanned at the full repetition rate of the FEL. In summary, we believe that simple and straightforward modifications will drastically improve the output, potentially providing valuable scientific returns to the ongoing efforts on 2D crystal snapshot diffraction at X-FELs.

4 Conclusions

Acquisition of diffraction data from single 2D crystals of proteins mounted on a solid support was previously shown to be feasible at X-FELs in diffract-before-destroy mode. Here, we demonstrated that exploiting the currently available X-ray pulse energies of about 2 mJ and merging data from multiple images makes it possible to unambiguosly identify diffraction peaks to a resolution of at least 7 Å. Multiple sampling of the same diffraction peak enhances the signal-to-noise ratio, which leads to enhanced resolution compared to the processing of single diffraction patterns. The above results relied on a limited number of single-crystal diffraction images, which leaves ample space for progress. The experiments were performed at room temperature, offering an obvious advantage with respect to techniques that need cryo-cooling to reduce radiation damage to the sample. The setup can be extended to pump-probe experiments, paving the way to structural dynamics studies of membrane proteins.

5 Acknowledgements

C.J.T., X.D.L. and G.F.X.S. acknowledge the Femtosecond and Attosecond Science and Technology (ETH FAST) Initiative in Switzerland. Part of the work was performed

under the auspices of the US Department of Energy by Lawrence Livermore National Laboratory under contract DE-AC52-07NA27344 and Pacific Northwest National Laboratory (operated by Battelle Memorial Institute) under Contract DE-AC05-76RL01830. Support was provided by the UCOP Lab Fee Program (award no. 118036), NIH grant number 5RC1GM091755, NSF award MCB-1021557 and NSF STC award 1231306, LLNL Lab-Directed Research and Development Project 012-ERD-031 and the PNNL Chemical Imaging Initiative. Part of the work was also funded by the Center for Biophotonics Science and Technology, a designated NSF Science and Technology Center managed by the University of California, Davis, under Cooperative Agreement No. PHY0120999.

The X-ray measurements were carried out at the Linac Coherent Light Source (LCLS) at SLAC National Accelerator Laboratory. LCLS is an Office of Science User Facility operated for the U.S. Department of Energy Office of Science by Stanford University.

References

[1] Rosenbaum, D. M., Rasmussen, S. G. F. & Kobilka, B. K. The structure and function of G-protein-coupled receptors. *Nature* **459**, 356–363 (2009).

[2] Deupi, X., Standfuss, J. & Schertler, G. Conserved activation paths in G-protein-coupled receptors. *Biochemical Society Transactions* **40**, 383–388 (2012).

[3] Fujiyoshi, Y. Electron crystallography for structural and functional studies of membrane proteins. *Journal of Electron Microscopy* **60**, S149–S159 (2011).

[4] Srivastava, S. K., Gayathri, S., Manjasetty, B. A. & Gopal, B. Analysis of Conformational Variation in Macromolecular Structural Models. *PLoS ONE* **7**, e39993 (2012).

[5] Unwin, P. N. T. & Henderson, R. Three-dimensional model of purple membrane obtained by electron microscopy. *Nature* **257**, 28–32 (1975).

[6] Kühlbrandt, W., Wang, D. N. & Fujiyoshi, Y. Atomic model of plant light-harvesting complex by electron crystallography. *Nature* **367**, 614–621 (1994).

[7] Schertler, G., Villa, C. & Henderson, R. Projection structure of rhodopsin. *Nature* **362**, 770–772 (1993).

[8] Gil, D., Carazo, J. M. & Marabini, R. On the nature of 2d crystal unbending. *Journal of Structural Biology* **156**, 546–555 (2006).

[9] Unwin, P. N. T. & Henderson, R. Molecular structure determination by electron microscopy of unstained crystalline specimens. *Journal of Molecular Biology* **94**, 425–440 (1975).

[10] Ceska, T. A. & Henderson, R. Analysis of high-resolution electron diffraction patterns from purple membrane labelled with heavy-atoms. *Journal of Molecular Biology* **213**, 539–560 (1990).

[11] Kunji, E. R., von Grunau, S., Oesterhelt, D. & Henderson, R. The three-dimensional structure of halorhodopsin to 5 Å by electron crystallography: A new unbending procedure for two-dimensional crystals by using a global reference structure. *Proceedings of the National Academy of Science of the USA* **97**, 4637–4642 (2000).

[12] Henderson, R. *et al.* Model for the structure of bacteriorhodopsin based on high-resolution electron cryo-microscopy. *Journal of Molecular Biology* **213**, 899–929 (1990).

[13] Gonen, T. *et al.* Lipid-protein interactions in double-layered two-dimensional AQP0 crystals. *Nature* **438**, 633–638 (2005).

[14] Henderson, R. The potential and limitations of neutrons, electrons and X-rays for atomic resolution microscopy of unstained biological molecules. *Journal of Molecular Biology* **28**, 171–193 (1995).

[15] Emma, P. *et al.* First lasing and operation of an ångstrom-wavelength free-electron laser. *Nature Photonics* **4**, 641–647 (2010).

[16] Pile, D. X-rays: First light from SACLA. *Nature Photonics* **5**, 456–457 (2011).

[17] Henderson, R. The structure of the purple membrane from *Halobacterium halobium*: Analysis of the X-ray diffraction pattern. *Journal of Molecular Biology* **93**, 123–138 (1975).

[18] Verclas, S. A. W. *et al.* X-ray diffraction from a single layer of purple membrane at the air/water interface. *Journal of Molecular Biology* **287**, 837–843 (1999).

[19] Boutet, S. *et al.* High-Resolution Protein Structure Determination by Serial Femtosecond Crystallography. *Science* **337**, 362–364 (2012).

[20] Spence, J. C. H., Weierstall, U., Fricke, T. T., Glaeser, R. M. & Downing, K. H. Three-dimensional diffractive imaging for crystalline monolayers with one-dimensional compact support. *Journal of Structural Biology* **144**, 209–218 (2003).

[21] Frank, M. *et al.* Femtosecond X-ray diffraction from two-dimensional protein crystals. *Submitted to International Union of Crystallography Journal* (2013).

[22] Boutet, S. & Williams, G. J. The Coherent X-ray Imaging (CXI) instrument at the Linac Coherent Light Source (LCLS). *New Journal of Physics* **12**, 035024 (2010).

[23] Baldwin, J. & Henderson, R. Measurement and evaluation of electron diffraction patterns from two-dimensional crystals. *Ultramicroscopy* **14**, 319–336 (1984).

[24] Henderson, R., Baldwin, J. M., Downing, K. H., Lepault, J. & Zemlin, F. Structure of purple membrane from *Halobacterium halobium*: recording, measurement and evaluation of the electron micrographs at 3.5 å resolution. *Ultramicroscopy* **19**, 147–178 (1990).

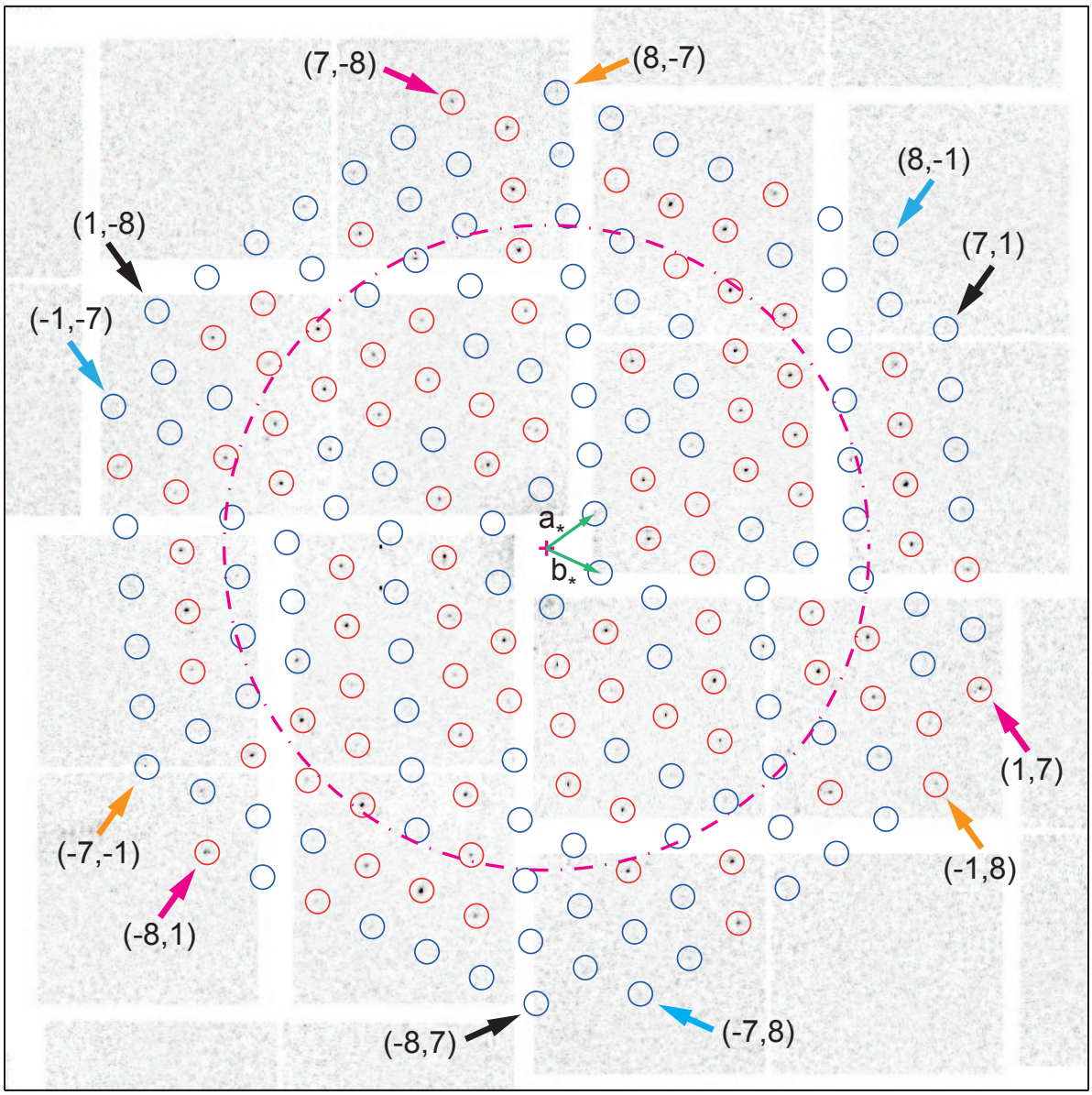

Figure 1: Example of a diffraction image from a single bR 2D crystal. The dashed ring corresponds to 10 Å resolution. The circles mark the positions of expected diffraction peaks at lower than 7 Åresolution. The precise orientation of the peak lattice was derived from the positions of the prominent, easily identifiable peaks encircled in red. The basis vectors (a_*, b_*) of the 2D reciprocal space lattice are shown as green arrows. The small arrows mark the position of peaks in the classes $((7,1))$ (black), $((1,7))$ (magenta), $((-7,-1))$ (orange) and $((-1,-7))$ (cyan), each class consisting of three equivalent peaks.

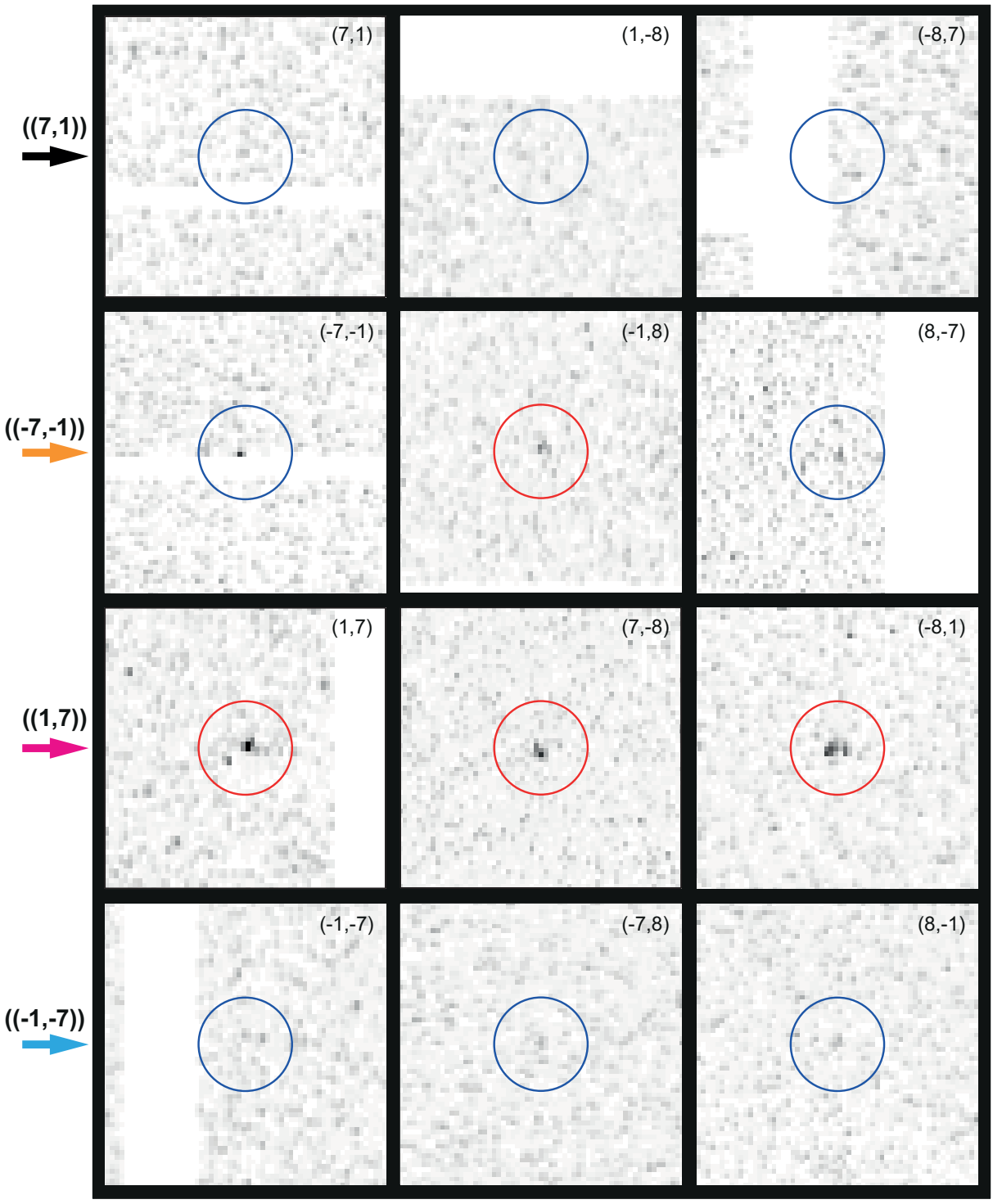

Figure 2: Magnifications of the diffraction image of Figure 1 around peak positions in classes $((7,1))$, $((-7,-1))$, $((1,7))$ and $((-1,-7))$. The color coding given by the arrows on the left is the same as in Figure 1.

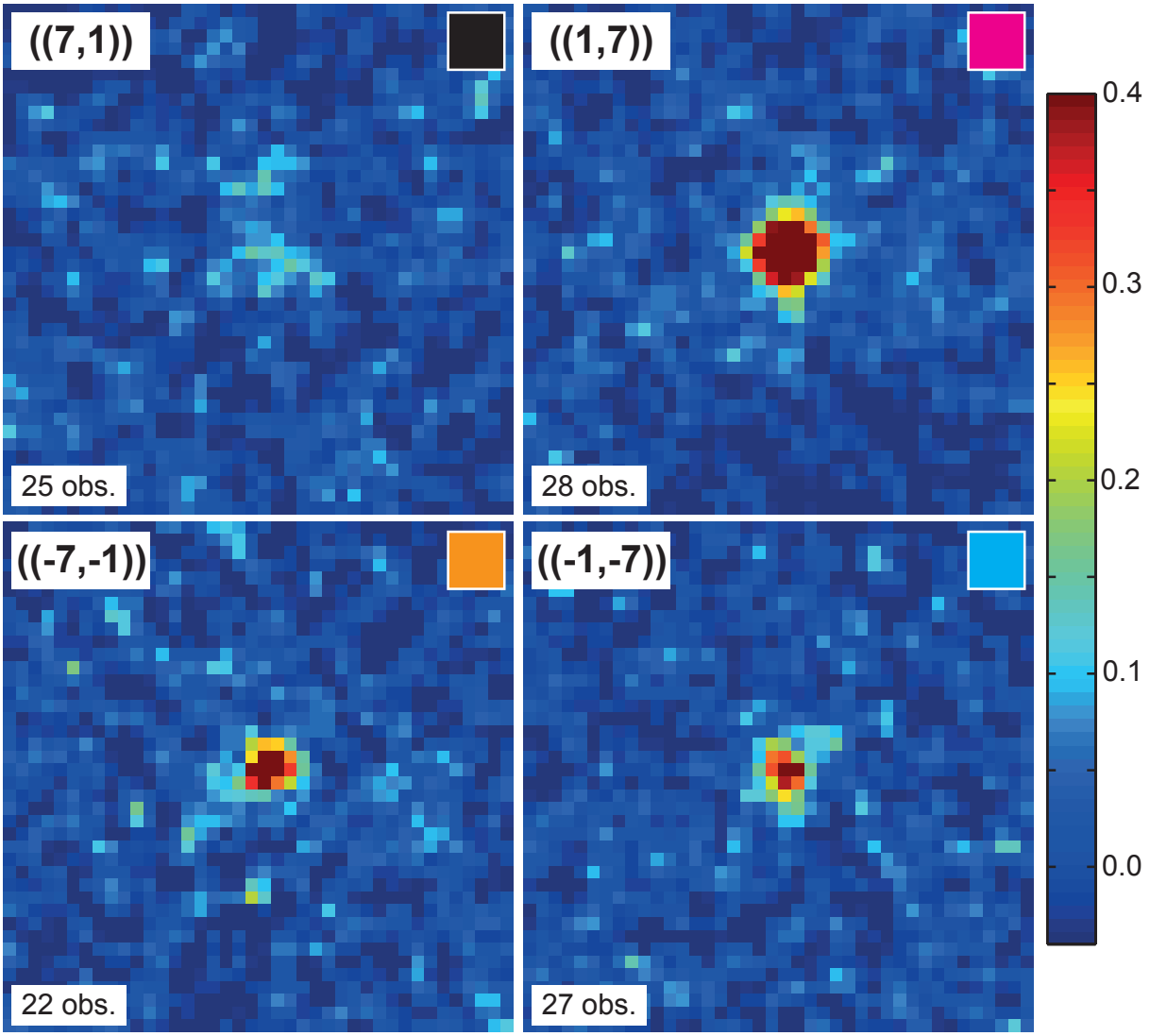

Figure 3: Examples of "image sector sums" (see text) for the four peak classes $((7,1))$, $((-7,-1))$, $((1,7))$ and $((-1,-7))$, all at 7.2 Å resolution. For each peak, the number of observations is indicated, and the color in the small box at the top right of each panel corresponds to that of the arrows in Figure 1. The intensity color scale is the same for all four panels. Maximum intensity is about 40 times the background noise, calculated as the average on all image sector sums of the local noise level measured away from the central peak region.